Journal of Non-Crystalline Solids 481 (2018) 202–207

Contents lists available at ScienceDirect

Journal of Non-Crystalline Solids

journal homepage: www.elsevier.com/locate/jnoncrysol

Short range order of $As_{40-x}Cu_xTe_{60}$ glasses

P. Jóvári[a,*], A. Piarristeguy[b], J.B. Vaney[b,c], I. Kaban[d], A. Zitolo[e], B. Beuneu[f], J. Bednarčik[g], G. Delaizir[h], J. Monnier[i], A.P. Gonçalves[j], C. Candolfi[c]

[a] Wigner Research Centre for Physics, Institute for Solid State Physics, H-1525 Budapest, POB 49, Hungary
[b] Institut Charles Gerhardt, UMR 5253 CNRS, CC1503, Université de Montpellier, Pl. E. Bataillon, F-34095 Montpellier cedex 5, France
[c] Institut Jean Lamour, UMR 7198 CNRS, Université de Lorraine, 2 allée André Guinier-Campus ARTEM, BP 50840, 54011 Nancy, France
[d] IFW Dresden, Institute for Complex Materials, Helmholtzstr. 20, 01069 Dresden, Germany
[e] Synchrotron SOLEIL, L'Orme des Merisiers, Saint Aubin, 91192 Gif sur Yvette, France
[f] Laboratoire Léon Brillouin, CEA-Saclay, 91191 Gif sur Yvette Cedex, France
[g] Deutsches Elektronen Synchrotron DESY, Notkestrasse 85, D-22603 Hamburg, Germany
[h] Science des Procédés Céramiques et de Traitements de Surface (SPCTS), UMR CNRS 7315, Centre Européen de la Céramique, Limoges, France
[i] Université Paris Est, ICMPE (UMR7182), CNRS, UPEC, 94320 Thiais, France
[j] C2TN, Instituto Superior Técnico, Universidade de Lisboa, Estrada Nacional 10, 2695-066 Bobadela, Portugal

ARTICLE INFO

Keywords:
Glass
Modeling
Reverse Monte Carlo
Diffraction
EXAFS

ABSTRACT

Short range order of $As_{40-x}Cu_xTe_{60}$ (x = 0, 10, 20, 25, 30) glasses was studied by neutron- and X-ray diffraction, combined with extended X-ray absorption fine structure (EXAFS) measurements at the K-edges of all components. Large-scale structural models were generated by fitting the experimental datasets simultaneously in the framework of the reverse Monte Carlo simulation technique. These simulations revealed that As and Te atoms bind to about 3 and 2 As/Te neighbors, respectively, both of which possess Cu neighbors. The Cu—Te bond length is 2.57 ± 0.02 Å while the Cu—As distance is as high as 2.86 ± 0.04 Å. The results further showed that besides As and Te, Cu atoms also bind to Cu. The total coordination number of Cu is significantly higher than 4 for the compositions x = 25 and 30.

1. Introduction

The structure of glasses in the As-Cu-Te system has been studied in the past by X-ray diffraction [1–4], neutron diffraction [5–8], as well as Raman and ^{65}Cu NMR spectroscopy [9]. Jimenez-Garay et al. [1–4] analyzed the short-range order of $Cu_xAs_{55-x}Te_{45}$ glasses with x = 10, 20 and 25 at.% Cu using X-ray diffraction. By using a theoretical expression of the area under the radial distribution function (RDF), these authors concluded that copper is fourfold coordinated in these glasses. For Cu-poor glasses (x = 5 and 15), however, only a correlation between electrical conduction and average coordination number has been reported.

On the other hand, Sonntag's group complemented these results by studying the line $Cu_xAs_{45-x}Te_{55}$ with x = 5, 10, 15 and 20 at.% Cu using neutron diffraction [5–7]. The analysis of the compositional dependence of the average coordination number indicated the existence of a critical composition, x_c = 6 below which the incorporation of copper does not lead to any significant increase in the coordination number of the chalcogen. Above this critical composition, the Te coordination increases linearly from 2 to 4 with increasing copper content. Fits of these experimental data by reverse Monte Carlo simulation [8] highlighted that Cu substitutes randomly for As (forming $CuTe_3$ pyramidal and $CuTe_4$ tetrahedral structural units as well as short Te-Cu-Te chains) and that the rigidity of the network increases with increasing Cu concentration. One of the intermediate glass compositions ($Cu_{4.8}As_{47.6}Te_{47.6}$), from the glasses previously mentioned, has been also investigated by using the method of isotopic substitution in neutron diffraction [9]. This experimental study showed that the addition of this small amount of copper does not significantly affect the short- or intermediate-range atomic ordering and the coordination number of Cu was found to be greater than four. A very recent study combining ^{65}Cu NMR and Raman spectroscopy performed on several lines of the Cu-As-Te glass system indicated the prevalence of tetrahedral $CuTe_4$ environments for the Cu atoms [10], while a study combining XANES and ab initio calculations [11] suggested that the valence of Te becomes positive upon adding Cu to As—Te glasses and electric conductivity is determined by the connectivity of Cu—Te and Te—Te bonds rather than Cu—Cu bonding.

As correlations in a three component system can be described by six partial pair correlation functions, the experimental determination of the

* Corresponding author.
E-mail address: jovari.pal@wigner.mta.hu (P. Jóvári).

http://dx.doi.org/10.1016/j.jnoncrysol.2017.10.046
Received 23 August 2017; Received in revised form 12 October 2017; Accepted 23 October 2017
Available online 08 November 2017
0022-3093/ © 2017 Elsevier B.V. All rights reserved.

short-range order in As-Cu-Te glasses is a challenging task. Diffraction techniques provide us with accurate *total* pair correlation functions but the separation of partial pair correlation functions requires element specific information already in the case of two-component glasses [12]. In the present case, the most straightforward way of getting element-specific information is to carry out extended X-ray absorption fine structure (EXAFS) measurements. Such information is particularly relevant to better understand the influence of the Cu content on the electrical and thermal transport properties of these glasses [13–16].

In this work, we report a detailed investigation on $As_{40-x}Cu_xTe_{60}$ glasses with the aim to determine the short range order through a combination of diffraction data and EXAFS measurements. The reverse Monte Carlo simulation technique [8,17] is used to generate large-scale structural models compatible with all experimental datasets. This method has already been proved to be very efficient for Ge-Sb-Te [18], Ge-Cu-Te [19] and Ge-As-Te glasses [20].

2. Experimental

2.1. Sample preparation

$Cu_xAs_{40-x}Te_{60}$ glasses with $0 \le x \le 30$ at.% Cu were prepared from 5N5 (99.9995% purity) copper pellets (Sigma-Aldrich), 4N5 (99.995% purity) tellurium (5NPlus) and 4N (99.99% purity) arsenic (Goodfellow). In all cases, 4 g of the elements weighted in stoichiometric quantities were loaded into a quartz ampoule (6 mm inner diameter) and sealed under vacuum (10^{-5} mbar). The ampoules were then heated at 850 °C with a 9 °C/h heating rate and kept at this temperature for 1 h. They were regularly rocked in the furnace to ensure homogenization. The ampoules were then cooled down to 600 °C, and further quenched into a "salt + ice + water" bath. For compositions with $x < 15$ and $x > 25$, the obtained materials were then crushed in small pieces, re-melted and quenched using the twin roller quenching technique (for more details see Refs [21,22]).

The amorphous nature of the materials was confirmed by performing X-ray diffraction using a PANalytical X'Pert diffractometer. A Cu (Kα) source (λ = 1.5406 Å) was used with an operating voltage of 40 kV and a beam current of 30–40 mA.

2.2. Measurements

High-energy X-ray diffraction (XRD) measurements were performed at the BW5 wiggler beamline [23] of the DORIS III positron storage ring operated at the HASYLAB/DESY (Hamburg, Germany). The energy of monochromatic synchrotron radiation was 100 keV (λ = 0.124 Å). Powder samples were placed into thin-walled (20 μm) quartz capillaries with outer diameter of 2 mm. The incident monochromatic beam cross section was set to 1 × 1 mm^2. The illumination time was around 15 s depending on the sample scattering power. About five independent scans on each sample were averaged to improve counting statistics. Scattered X-ray photons were collected using a MAR345 imaging plate detector (2300 × 2300 pixels, with pixel size of 150 × 150 μm^2). LaB_6 standard was used to calibrate the sample-to-detector distance and tilt of the imaging plate relative to the beam path. The background intensity was subtracted directly from the measured 2D XRD patterns, and the resulting patterns were integrated to *k*-space using the software package FIT2D [24]. The integrated data were corrected for polarization, sample absorption, fluorescence contribution, and inelastic (Compton) scattering using standard procedures described in [25].

Neutron diffraction measurements were carried out at the 7C2 diffractometer of Laboratoire Léon Brillouin (Gif-sur-Yvette, France). Powdered samples were filled into vanadium containers (wall thickness: 0.1 mm, diameter: 6 mm). The wavelength of incident radiation was 0.72 Å. Scattered intensities were measured by the new ^{3}He detector consisting of 256 tubes. Raw data were corrected for detector efficiency and background scattering.

The EXAFS measurements were carried out at room temperature at the SAMBA beamline of Soleil Synchrotron (Saclay, France). The beamline is equipped with a sagittally focusing Si 220 monochromator and two Pd-coated collimating/focusing mirrors to remove higher harmonics. Samples were pelletized as disks of 10 mm diameter with 1 mm thickness using cellulose powder as a binder. As and Te k-edges spectra were collected in transmission mode, while Cu K-edge spectra were recorded in fluorescence geometry to get a better signal/noise ratio, using a 35-elements Ge detector (Canberra). The X-ray absorption cross sections and fluorescence intensities were converted to $\chi(k)$ by standard procedures of data reduction using the program VIPER [26]. Raw χ(k) data were filtered in two steps: first $k^3\chi(k)$ was forward Fourier-transformed into r-space using a Kaiser-Bessel window ($\alpha = 1.5$). The k-range of transformation was about 1.9 $Å^{-1}$–14 $Å^{-1}$ for all edges. The resulting *r*-space data were backtransformed using a rectangular window (the r-space ranges are 1.4 Å–2.9 Å, 1.1 Å–2.8 Å, 1.6 Å–3.0 Å for As, Cu and Te EXAFS data, respectively).

2.3. Reverse Monte Carlo Simulation (RMC)

The reverse Monte Carlo simulation technique is a method for creating large real-space models compatible with diffraction and EXAFS measurements. The central quantities of the method are the partial pair correlation functions, which connect experiment and modeling.

The output of a diffraction measurement is the structure factor $S(q)$, which is the combination of $S_{ij}(q)$ partial structure factors (for details see [27–29]):

$$S(q) = \sum_{i \le j} w_{ij} S_{ij}(q) \tag{1}$$

For X-ray and electron diffraction the weights are the functions of q, while for neutron diffraction they do not depend on q. The partial structure factors are related to the $g_{ij}(r)$ partial pair correlation functions via the following transformation:

$$q(S_{ij}(q) - 1) = 4\pi\rho \int r(g_{ij}(r) - 1)\sin(qr)dr \tag{2}$$

Here ϱ is the number density of the sample (given in atom/$Å^{-3}$ if the momentum transfer q is given in $Å^{-1}$). The total pair correlation function $G(r)$ can be obtained from the structure factor by Fourier-transformation:

$$r(G(r) - 1) = \frac{1}{2\pi^2\rho} \int q(S(q) - 1)\sin(qr)dr \tag{3}$$

In case of neutron diffraction where the w_{ij} weighting factors do not depend on q the total pair correlation function can also be obtained by the real space analog of Eq. (1):

$$G(r) = \sum_{i \le j} w_{ij} g_{ij}(r) \tag{4}$$

For X-ray and electron diffraction the weights depend on q therefore the order of summation (Eq. (1)) and integration (Eq. (3)) cannot be changed.

In the simulation all real-space quantities ($G(r)$, $g_{ij}(r)$) are calculated over a discrete *r*-space grid. To be able to reproduce diffraction data over the experimental window the grid size cannot be larger than δr, the resolution of the experiment. The latter is given by the sampling theorem:

$$\delta r = \frac{\pi}{q_{\max} - q_{\min}} \tag{5}$$

The resolution of an experiment also determines n, the number of independent fitting parameters over an *r*-space region with a width of ΔR:

$$n \approx \frac{\Delta R}{\delta r} = \frac{\Delta R(q_{\max} - q_{\min})}{\pi} \quad (6)$$

Our aim is to resolve the first peaks of the partial pair correlation functions. These peaks merge into a single peak of the total pair correlation function between ~2.3 Å and ~3.2 Å. As δr is about 0.2 Å for the neutron diffraction data the number of independent fitting parameters is about 5 for this measurement. For X-ray diffraction $n \approx 7$ due to the higher q_{max} value.

For EXAFS the number of independent fitting parameters is estimated by the following equation [30]:

$$n \approx \frac{2\Delta R(k_{\max} - k_{\min})}{\pi} \quad (7)$$

Here ΔR is the width of the main peak of the module of Fourier-transformed EXAFS signal while k_{max}-k_{min} is the fitted experimental window, similarly to the case of diffraction data. As ΔR is usually around 1.5 Å while k_{max}-k_{min} is around 6–8 $Å^{-1}$, the number of relevant fitting parameters is about 7 for each EXAFS spectrum.

The sum of relevant independent parameters for five measurements (neutron- and X-ray diffraction, As-, Cu- and Te K-edge EXAFS) is about 33. This is an upper estimate of the total number of relevant independent parameters as some parameters are 'shared' by more measurements. For example, both diffraction datasets as well as Te and As EXAFS spectra contain information on the mean As—Te distance and coordination number.

In the simplest case a symmetric peak can be characterized by three parameters (center, height, area). If all six partial pair correlation functions have symmetric first peaks then the number of relevant fitting parameters is 18. As some peaks may not be symmetric, this value can be regarded as a lower estimate for the number of fitting parameters. The actual value is thus between 18 and 33. The sum of grid points of the partial pair correlation functions in the nearest neighbour region is around 25–29 (some minimum positions shift with composition). This number proved to be sufficient to fit all measurements. We will also see that if the number of parameters is reduced (e.g. by increasing the As—Cu cut off) then the fit quality deteriorates, showing that for $As_{20}Cu_{20}Te_{60}$ and $As_{15}Cu_{25}Te_{60}$ the number of independent fitting parameters matches up the number of grid points in the nearest neighbour region.

For $As_{10}Cu_{30}Te_{60}$ and $As_{30}Cu_{10}Te_{60}$ there are only four measurements available. Due to the lack of Cu EXAFS data the uncertainty of Cu-related structural parameters of $As_{30}Cu_{10}Te_{60}$ (e.g. N_{Cu}, the average total coordination number of Cu – see Table 2) was higher but it did not affect the conclusions. No higher uncertainty was observed for the Te-related structural parameters of $As_{10}Cu_{30}Te_{60}$, which were obtained without Te EXAFS data. The reason is most likely the high concentration of Te that makes the other four datasets sensitive to Te-related structural parameters.

The *rmcpp* code [17] was used to fit neutron diffraction, X-ray diffraction and EXAFS datasets simultaneously. Each simulation was started from a random configuration. Simulation boxes contained 20,000 atoms. The number densities of the $As_{40-x}Cu_xTe_{60}$ samples (x = 10, 25, 30) were determined by inter- or extrapolating the number densities of $As_{40}Te_{60}$ and $As_{20}Cu_{20}Te_{60}$ from Borisova [31]. Sample compositions, number densities and datasets fitted are listed in Table 1. X-ray atomic form factors were taken from Waasmaier and Kirfel [32]. EXAFS backscattering amplitudes and phases needed to calculate the model $\chi(k)$ function were obtained by the FEFF8.4 code [33].

The maximum random displacement of atoms in a move was 0.15 Å along each coordinate. The minimum interatomic distances (cut offs) for As—As, As—Cu, As—Te, Cu—Cu, Cu—Te and Te—Te pairs were 2.3 Å, 2.65 Å, 2.4 Å, 2.35 Å, 2.3 Å and 2.5 Å, respectively.

3. Results

Fig. 1 shows the experimental and RMC simulated structure factors and $k^3\chi(k)$ functions of $As_{20}Cu_{20}Te_{60}$ obtained by fitting simultaneously the five measurements. As seen in this figure, the computed functions reproduce very well the X-ray diffraction and EXAFS measurements at the K-edges of As, Cu and Te. It should be noted that no coordination constraints were used during the simulations. Partial pair correlation functions of the same composition can be seen in Fig. 2 while coordination numbers and nearest neighbour distances for all compositions investigated are given in Tables 2 and 3.

It can be observed that the sum of average As—As and As—Te coordination numbers is close to 3 for $x \leq 25$. For $x = 30$, the uncertainty in the As-related structural parameters is somewhat higher due to the relatively low concentration of As.

While the average number of both Te and As atoms around Te changes significantly (Table 2), the sum of average Te—Te and Te—As coordination numbers is very close to 2 in all cases. It can thus be concluded that the covalent network of As and Te atoms remains – at least topologically – intact upon adding Cu. We note here again that no coordination constraints were used during the simulations; therefore, the above finding follows directly from the measured data.

The average coordination number of Cu atoms is around 4 for $x \leq 20$ but becomes significantly higher for x = 25 and 30. The increase is due to the average Cu—Cu coordination number, which is as high as 3.11 ± 0.7 for x = 30. The average number of Te atoms around Cu is about 2–2.5 over the whole composition range investigated. Cu—As bonds can also be found in the As-Cu-Te glasses investigated. The corresponding coordination number decreases with increasing x, in line with the expectations. The presence of Cu—As bonds has been proven by dedicated simulation runs. In Figs. 3 and 4, we compare the $As_{20}Cu_{20}Te_{60}$ As K-edge fits and the Cu—Cu and Cu—As partial pair correlation functions obtained with and without Cu—As bonds. Two observation can be made here: i) the fit quality worsens upon eliminating Cu—As bonding, ii) a secondary Cu—Cu peak appears in the Cu—Cu partial pair correlation function to compensate for the lack of the Cu—As peak. This secondary Cu—Cu peak is necessary to maintain at least the Cu K-edge EXAFS fit quality. The above signs indicate the formation of Cu—As pairs. The nature of Cu—As bonding is not clear, however. The Cu—As distance is around 2.89 Å, which is much longer than for example the mean Cu-As/Se distance (2.40 ± 0.02 Å) found in As-Cu-Se glasses by isotopic substitution [34].

Molar volumes of $As_{50-x/2}Cu_xTe_{50-x/2}$ and $As_{50-x/2}Ge_xTe_{50-x/2}$ glasses have been compared in [9]. The results showed that the molar volume of As-Cu-Te glasses decreases with increasing x (from about 17.7 cm^3/mol at x = 5 to 15.8 cm^3/mol at x = 20) while the reported molar volume of As-Ge-Te glasses fluctuates around a constant value (~18.1 cm^3/mol) over the same composition range. This difference also suggests that unlike Ge, Cu does not build in the As—Te network but occupies the volume between As/Te atoms.

Table 1
Sample compositions, number densities (in $Å^{-3}$) and datasets fitted in reverse Monte Carlo simulation.

Composition	$As_{40}Te_{60}$	$As_{30}Cu_{10}Te_{60}$	$As_{20}Cu_{20}Te_{60}$	$As_{15}Cu_{25}Te_{60}$	$As_{10}Cu_{30}Te_{60}$
Number density	0.0311	0.0332	0.0356	0.0369	0.0381
Datasets fitted	nd, xrd, As, Te	nd, xrd, As, Te	nd, xrd, As, Cu, Te	nd, xrd, As, Cu, Te	nd, xrd, As, Cu

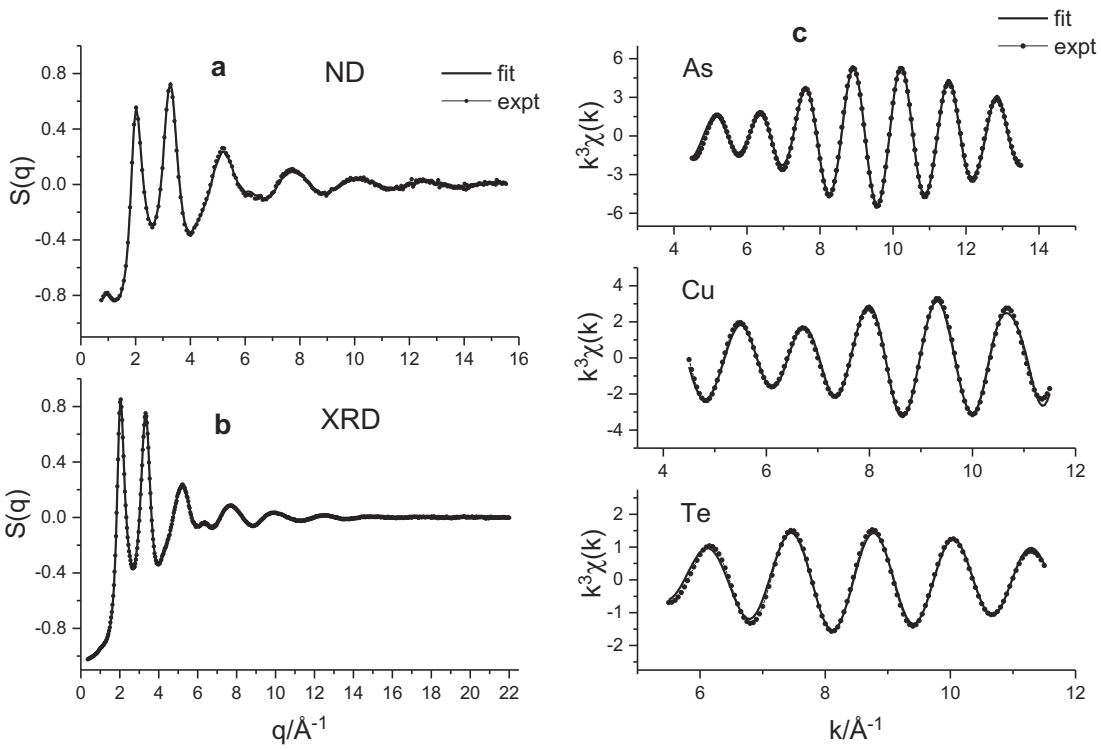

Fig. 1. Experimental (circles) and fitted (thick lines) curves of $As_{20}Cu_{20}Te_{60}$ glass obtained by the simultaneous RMC modeling of the five measurements: (a) neutron diffraction, (b) X-ray diffraction and (c) EXAFS measurements at the K-edges of As, Cu and Te.

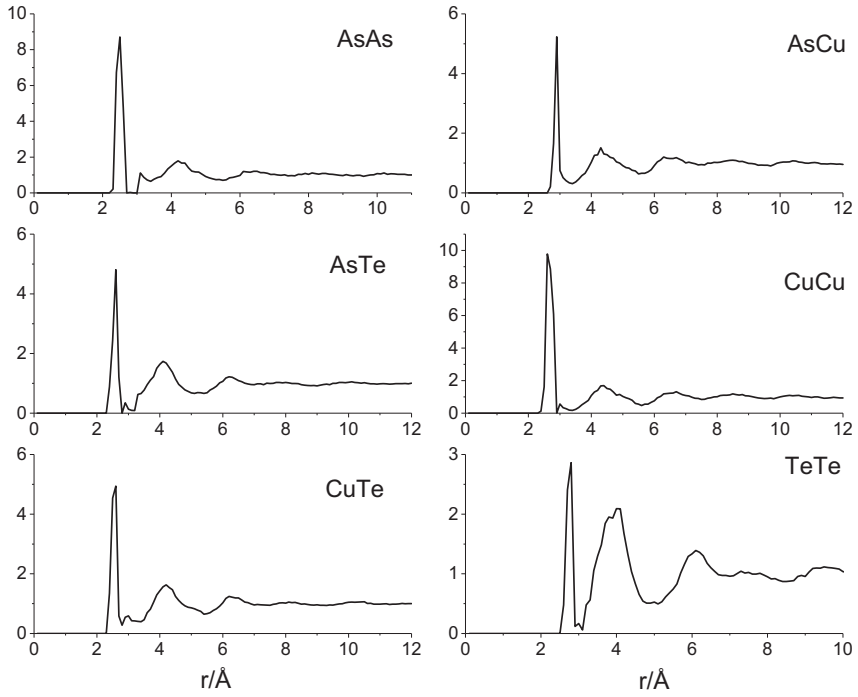

Fig. 2. Partial pair correlation functions of $As_{20}Cu_{20}Te_{60}$ glass obtained by the simultaneous RMC modeling of the five measurements.

3.1. Comparison with other amorphous tellurides

The structure of an amorphous $GeCu_2Te_3$ thin film was studied recently by fitting X-ray diffraction and EXAFS measurements using the reverse Monte Carlo simulation technique [19]. It was found that the total average coordination numbers of Cu and Te are equally around 4. The high coordination number of Te is only partly due to Te—Cu bonds (N_{TeCu} = 1.39 ± 0.2). The sum of Te—Te and Te—Ge average coordination numbers (2.71 ± 0.4) is also significantly higher than 2 showing that Cu strongly modifies the covalent network of Ge and Te atoms. This is in stark contrast with the case of $As_{40-x}Cu_xTe_{60}$ glasses where the sum of Te—Te and Te—As coordination numbers remains close to 2 over the whole composition range investigated. The mean Cu—Cu distance (2.58 ± 0.03 Å) is significantly shorter in amorphous $GeCu_2Te_3$ than in the As-Cu-Te glasses investigated (2.67–2.70 Å).

Short range order of $Ge_{15}Cu_5Te_{80}$ and $Ge_{15}Cu_8Te_{77}$ was investigated by X-ray diffraction, Ge- and Cu K-edge EXAFS measurements [35]. It was found that the total coordination number of Te is significantly

Table 2
N_{ij} coordination numbers in As-Cu-Te glasses obtained by fitting simultaneously diffraction structure factors and EXAFS signals with the reverse Monte Carlo modeling technique.

	$As_{40}Te_{60}$	$As_{30}Cu_{10}Te_{60}$	$As_{20}Cu_{20}Te_{60}$	$As_{15}Cu_{25}Te_{60}$	$As_{10}Cu_{30}Te_{60}$
N_{AsAs}	1.82 ± 0.3	1.07 ± 0.3	1.13 ± 0.3	1.18 ± 0.3	0.79 ± 0.3
N_{AsCu}	–	0.37 ± 0.2	0.71 ± 0.25	0.85 ± 0.25	0.51 ± 0.3
N_{AsTe}	1.34 ± 0.3	1.58 ± 0.3	1.80 ± 0.3	1.94 ± 0.4	2.76 ± 0.6
N_{CuAs}	–	1.11 ± 0.6	0.71 ± 0.25	0.51 ± 0.15	0.17 ± 0.1
N_{CuCu}	–	1.07 ± 0.6	1.69 ± 0.5	1.83 ± 0.5	3.11 ± 0.7
N_{CuTe}	–	2.32 ± 0.6	2.01 ± 0.6	2.46 ± 0.6	2.17 ± 0.5
N_{TeAs}	0.89	0.79 ± 0.25	0.60 ± 0.2	0.49 ± 0.2	0.46 ± 0.1
N_{TeCu}	–	0.39 ± 0.2	0.67 ± 0.2	1.03 ± 0.25	1.08 ± 0.25
N_{TeTe}	1.01	1.14 ± 0.2	1.43 ± 0.2	1.44 ± 0.2	1.65 ± 0.2
$N_{AsAs} + N_{AsTe}$	3.16 ± 0.3	2.65 ± 0.3	2.93 ± 0.3	3.12 ± 0.3	3.55 ± 0.6
$N_{TeAs} + N_{TeTe}$	1.90 ± 0.2	1.93 ± 0.2	2.03 ± 0.2	1.93 ± 0.2	2.11 ± 0.2
N_{As}	3.16 ± 0.3	3.02 ± 0.3	3.64 ± 0.3	3.97 ± 0.3	4.06 ± 0.6
N_{Cu}	–	4.50 ± 1.0	4.41 + 0.5	4.80 ± 0.5	5.45 ± 0.6
N_{Te}	1.90 ± 0.2	2.32 ± 0.2	2.70 ± 0.2	2.96 ± 0.2	3.19 ± 0.3

Table 3
r_{ij} nearest neighbour distances (in Å) in amorphous As-Cu-Te alloys obtained by fitting simultaneously diffraction structure factors and EXAFS signals with the reverse Monte Carlo modeling technique.

	$As_{40}Te_{60}$	$As_{30}Cu_{10}Te_{60}$	$As_{20}Cu_{20}Te_{60}$	$As_{15}Cu_{25}Te_{60}$	$As_{10}Cu_{30}Te_{60}$
r_{AsAs}	2.45 ± 0.02	2.46 ± 0.02	2.49 ± 0.02	2.51 ± 0.03	2.48 ± 0.03
r_{AsCu}	–	2.87 ± 0.05	2.89 ± 0.03	2.85 ± 0.03	2.87 ± 0.03
r_{AsTe}	2.58 ± 0.02	2.60 ± 0.03	2.58 ± 0.03	2.59 ± 0.03	2.57 ± 0.03
r_{CuCu}	–	2.70 ± 0.05	2.67 ± 0.03	2.67 ± 0.03	2.69 ± 0.03
r_{CuTe}	–	2.59 ± 0.04	2.55 ± 0.03	2.54 ± 0.03	2.59 ± 0.03
r_{TeTe}	2.75 ± 0.02	2.76 ± 0.02	2.76 ± 0.02	2.74 ± 0.02	2.76 ± 0.02

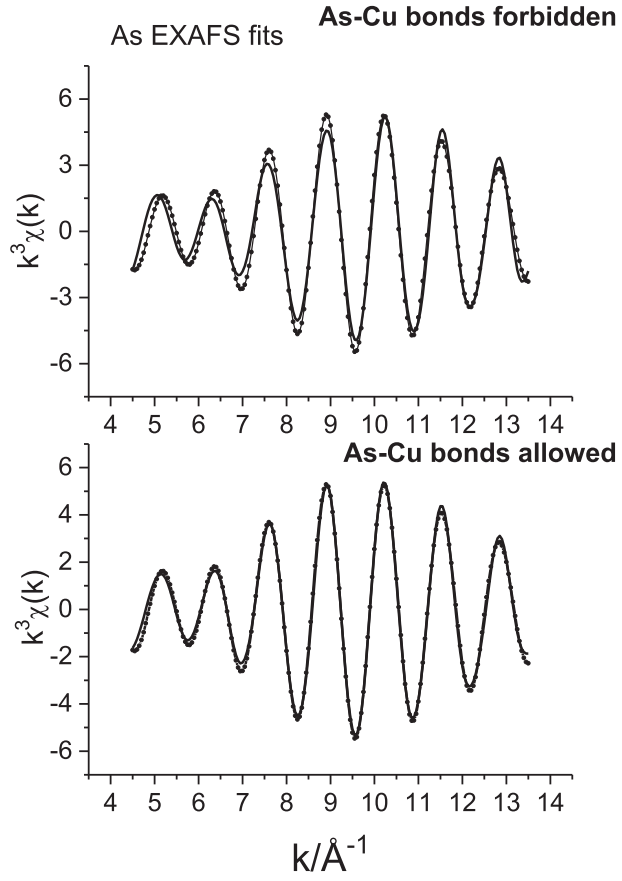

Fig. 3. Comparison of As K-edge EXAFS fits obtained with and without As-Cu bonds.

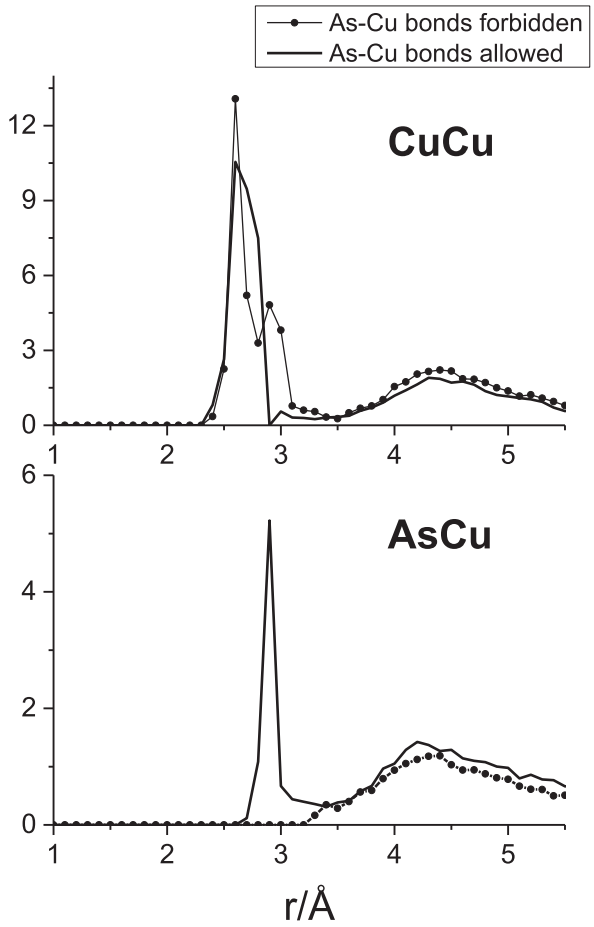

Fig. 4. Comparison of As-Cu and Cu-Cu partial pair correlation functions obtained with and without As-Cu bonds.

higher than 2 in $Ge_{15}Cu_8Te_{77}$. The Cu−Te distance is 2.56 ± 0.02 Å, which is in good agreement with the values found in $As_{40-x}Cu_xTe_{60}$ glasses. On the other hand, the Cu−Cu distance was found to be significantly larger in $Ge_{15}Cu_8Te_{77}$ than in $As_{40-x}Cu_xTe_{60}$ glasses (2.80 ± 0.02 Å and 2.67–2.70 Å, respectively). The average coordination number of Cu is 3.4 ± 1.0 in $Ge_{15}Cu_8Te_{77}$. The relatively large uncertainty stems from the low concentration of Cu.

The total average coordination number of Cu was found to be 4.54 ± 0.3 in 0.9($Ge_5As_{55}Te_{40}$)-0.1Cu (GATC) glass [36]. Besides Cu−Te and Cu−Cu bonds, As−Cu bonding was also found to be significant in this system (N_{CuAs} = 1.40 ± 0.4). It should be noted that the Cu−As distance is significantly shorter in GATC than in the As-Cu-Te glasses investigated in this study (2.76 ± 0.02 Å vs 2.85–2.89 Å), suggesting that this distance may be sensitive to the average interatomic distances in the $Ge_5As_{55}Te_{40}$, which 'rescales' the volume available for Cu atoms.

4. Conclusions

Atomic level structure in $As_{40-x}Cu_xTe_{60}$ (x = 0, 10, 20, 25, 30) glasses was studied by the reverse Monte Carlo simulation technique by fitting simultaneously neutron- and X-ray diffraction as well as EXAFS measurements. It was found that similarly to binary As_xTe_{100-x} ($x \leq 50$) glasses, As and Te atoms bind to 3 and 2 As/Te neighbors, respectively. Both As and Te have Cu neighbors already in $As_{30}Cu_{10}Te_{60}$. The Cu−Te bond length is about 2.57 ± 0.03 Å, while the Cu−As distance is around 2.86 ± 0.04 Å. Besides As and Te, Cu atoms also bind to Cu. The total coordination number of Cu is around 4 for x = 10 and 20 and increases to 5.45 ± 0.6 for x = 30 due to the increasing Cu−Cu coordination number.

Acknowledgments

P.J. was supported by NKFIH (National Research, Development and Innovation Office) Grant No. SNN 116198. Financial support from the French National Agency (ANR) in the frame of the program «PROGELEC» (verre thermo-générateur «VTG») is acknowledged (project identifier ANR-11-PRGE-0010). We acknowledge Synchrotron SOLEIL (Gif-sur Yvette, France) for provision of synchrotron radiation facilities at beamline SAMBA (proposal number 20140279).

The assistance of Claudia Pantalei during the neutron diffraction experiment is greatly acknowledged.

References

[1] E. Marquez, J. Vázquez, N. de la Rosa-Fox, P. Villares, R. Jimenez-Garay, J. Mater. Sci. 23 (1988) 1388.
[2] C. Wagner, J. Vazquez, P. Villares, R. Jimenez-Garay, Mater. Lett. 16 (1993) 243.
[3] C. Wagner, J. Vázquez, P. Villares, R. Jimenez-Garay, J. Mater. Sci. 29 (1994) 3316.
[4] C. Wagner, J. Vázquez, P. Villares, R. Jimenez-Garay, Il Nuovo Cimento 16D (3) (1994) 233.
[5] N. Zotov, R. Jimenez-Garay, F. Bellido, M. Dominguez, A.C. Hannon, R. Sonntag, Physica B 424 (1997) 234–236.
[6] N. Zotov, F. Bellido, M. Dominguez, R. Jimenez-Garay, A.C. Hannon, R. Sonntag, J. Phys. Chem. Solids 58 (10) (1997) 1625.
[7] N. Zotov, F. Bellido, M. Dominguez, A.C. Hannon, R. Sonntag, Physica B 463 (2000) 276–278.
[8] R.L. McGreevy, L. Pusztai, Mol. Simul. 1 (1988) 359.
[9] J.C. Wasse, I. Petri, P.S. Salmon, J. Phys. Condens. Matter 13 (2001) 6165.
[10] P. Lucas, G.J. Coleman, D.C. Kaseman, Z. Yang, I. Hung, Z. Gan, S. Sen, J. Non-Cryst. Solids 432 (2016) 527.
[11] S. B Srinivasan, C. Cui, A. Prestipino, C. Gellé, S. Boussard-Pledel, A. Ababou-Girard, B. Trapananti, S. Bureau, J. Di Matteo, Phys. Chem. C 121 (2017) 14045.
[12] P. Jóvári, S.N. Yannopoulos, I. Kaban, A. Kalampounias, I. Lischynskyy, B. Beuneu, O. Kostadinova, E. Welter, A. Schöps, J. Chem. Phys. 129 (2008) 214502.
[13] J.B. Vaney, G. Delaizir, E. Alleno, O. Rouleau, A. Piarristeguy, J. Monnier, C. Godart, M. Ribes, R. Escalier, A. Pradel, A.P. Gonçalves, E.B. Lopes, G.J. Cuello, P. Ziolkowski, E. Müller, C. Candolfi, A. Dauscher, B. Lenoir, J. Mater. Chem. A 1 (2013) 8190.
[14] J.B. Vaney, A. Piarristeguy, A. Pradel, E. Alleno, B. Lenoir, C. Candolfi, A. Dauscher, A.P. Gonçalves, E.B. Lopes, G. Delaizir, J. Monnier, M. Ribes, C. Godart, J. Solid State Chem. 203 (2013) 212.
[15] A.P. Gonçalves, E.B. Lopes, G. Delaizir, J.B. Vaney, B. Lenoir, A. Piarristeguy, A. Pradel, J. Monnier, P. Ochin, C. Godart, J. Solid State Chem. 193 (2012) 26.
[16] J.-B. Vaney, J. Carreaud, C. Morin, G. Delaizir, A. Piarristeguy, M. Colas, J. Cornette, R. Le Parc, E. Alleno, J. Monnier, M. Ribes, R. Escalier, A. Pradel, A.P. Gonçalves, E. Branco Lopes, C. Candolfi, B. Lenoir, J. Am. Ceram. Soc. 100 (2017) 2840.
[17] O. Gereben, P. Jóvári, L. Temleitner, L. Pusztai, J. Optoelectron. Adv. M. 9 (2017) 3021.
[18] P. Jóvári, I. Kaban, J. Steiner, B. Beuneu, A. Schöps, A. Webb, Phys. Rev. B77 (2008) 035202.
[19] P. Jóvári, Y. Sutou, I. Kaban, Y. Saito, J. Koike, Scr. Mater. 68 (2013) 122.
[20] P. Jóvári, P. Lucas, Z. Yang, B. Bureau, I. Kaban, B. Beuneu, J. Bednarčik, J. Am. Ceram. Soc. 97 (2014) 1625.
[21] A. Pradel, T. Pagnier, M. Ribes, Solid State Ionics 17 (1985) 147.
[22] A.A. Piarristeguy, E. Barthélémy, M. Krbal, J. Frayret, C. Vigreux, A. Pradel, J. Non-Cryst. Solids 355 (2009) 2088.
[23] R. Bouchard, D. Hupfeld, T. Lippmann, J. Neuefeind, H.B. Neumann, H.F. Poulsen, U. Rütt, T. Schmidt, J.R. Schneider, J. Süssenbach, M. von Zimmermann, J. Synchrotron Radiat. 5 (1988) 90.
[24] A.P. Hammersley, S.O. Svensson, M. Hanfland, A.N. Fitch, D. Häusermann, High Pressure Res. 14 (1996) 235.
[25] H.F. Poulsen, J. Neuefeind, H.-B. Neumann, J.R. Schneider, M.D. Zeidler, J. Non-Cryst. Solids 188 (1995) 63.
[26] K.V. Klementev, J. Phys. D. Appl. Phys. 34 (2001) 209.
[27] G.J. Cuello, J. Phys. Condens. Matter 20 (2008) 244109.
[28] D.A. Keen, J. Appl. Crystallogr. 34 (2001) 172.
[29] H.E. Fischer, A.C. Barnes, P.S. Salmon, Rep. Prog. Phys. 69 (2006) 233.
[30] P.A. Lee, P.H. Citrin, P. Eisenberger, B.M. Kincaid, Rev. Mod. Phys. 53 (1981) 769.
[31] Z.U. Borisova, Glassy Semiconductors, Plenum, New York, 1981.
[32] D. Waasmaier, A. Kirfel, Acta Cryst. A 51 (1995) 416.
[33] A.L. Ankudinov, B. Ravel, J.J. Rehr, S.D. Conradson, Phys. Rev. B 58 (1988) 7565.
[34] S. Xin, J. Liu, P. Salmon, Phys. Rev. B 78 (2008) 064207.
[35] L. Rátkai, A.P. Gonçalves, G. Delaizir, C. Godart, I. Kaban, B. Beuneu, P. Jóvári, Solid State Commun. 151 (2011) 1524.
[36] P. Jóvári, P. Lucas, Z. Yang, B. Bureau, I. Kaban, B. Beuneu, C. Pantalei, J. Bednarčik, J. Journal of Non-Crystalline Solids 433 (2016) 1.